Resonant inverse photoemission in cerium-based materials

M. Grioni,* P. Weibel,† D. Malterre,‡ and Y. Baer
Institut de Physique, Université de Neuchâtel, CH-2000 Neuchâtel, Switzerland

L. Duò
Istituto Nazionale di Fisica della Materia-Dipartimento di Fisica, Politecnico di Milano, Piazza L. da Vinci 32, I-20133 Milano, Italy
(Received 3 July 1996)

The Ce $4f$ part of the electron addition spectra of cerium compounds is selectively and resonantly enhanced when the excitation energy coincides with the Ce $3d \rightarrow 4f$ ($M_{4,5}$) absorption edge. Different spectral features, corresponding to $4f^1$ and $4f^2$ configurations in the final state, exhibit distinct resonance profiles. The relative intensities of the f^1 and f^2 resonances may vary by as much as a factor of 50, according to the strength of the hybridization between $4f$ and conduction-band states. At resonance the spectral line shape is unambiguously modified when the temperature is varied across the characteristic Kondo temperature.
[S0163-1829(97)05204-1]

I. INTRODUCTION

Metallic cerium-based systems offer a classic example of strongly correlated electrons (the Ce $4f$ electrons) on the verge of localization. Many of the physical properties of these systems reflect the peculiar nature of the $4f$ states and the existence of a material-dependent low-energy scale or, equivalently, characteristic temperature (the Kondo temperature T_K). The magnetic susceptibility, for instance, exhibits a Curie-Weiss behavior for $T \gg T_K$, but Pauli paramagnetism for $T \ll T_K$.

Electron spectroscopies, in particular photoemission spectroscopy (PES) and inverse photoemission spectroscopy [(IPES), also known as bremsstrahlung isochromat spectroscopy (BIS)] provide direct evidence of the strength of correlations in these materials.[1] Unlike conventional transport or magnetic or specific-heat measurements, which are sensitive only to the low-energy spin fluctuations, the high-energy data reflect both low- (spin) and high-energy (charge) degrees of freedom. In principle, the combined electron removal (PES) and addition (IPES) spectra define the one-particle properties of an electron system and are therefore quite complementary. In practice, mainly for technical reasons, PES is much more widely used than IPES. Especially in Ce materials, however, IPES has a paramount importance since it can directly probe the mostly unoccupied $4f$ states.

Experimental PES and IPES spectra of Ce materials always contain overlapping contributions from $4f$ and conduction-band states, which are often difficult to disentangle. Uncertainties in the determination of the $4f$ spectral function are an obstacle to a quantitative exploitation of both techniques. In PES it is customary to compare measurements performed at various photon energies and to exploit the different energy-dependent photoionization cross sections for the $4f$ and the conduction-band electrons. This strategy is most effective when photon energies are varied across the $4d \rightarrow 4f$ ($N_{4,5}$) or $3d \rightarrow 4f$ ($M_{4,5}$) excitation thresholds, where the $4f$ cross section presents resonant enhancements.[2–7] Similar arguments do apply to the inverse photoemission transition matrix elements, but the energy dependence of the cross section is seldom exploited in IPES.[8]

Recently[9] we have shown that it is possible to perform state-of-the-art IPES measurements of cerium systems at the Ce M_5 threshold and we have described some of the advantages of this resonant IPES (RIPES) technique. Our work follows previous results by Liefeld, Burr, and Chamberlain,[10] by Riehle,[11] and by Shulakov, Zimkina, and Formichev,[12] which experimentally established the existence of resonances in IPES. We have taken advantage of subsequent progress in vacuum technology and in the detection of soft x rays and we have designed a dedicated RIPES spectrometer that fulfills the stringent UHV conditions required by the high reactivity of Ce compounds.[13] In this paper we present the results of an investigation of selected compounds spanning the entire range of physical properties of metallic Ce-based materials. We will not provide a detailed analysis of any particular material, but rather present a large data set, showing some systematic trends as well as the possibilities offered by RIPES. We will show that RIPES provides some information on the spectral properties of these materials.

The paper is organized as follows. In Sec. II we discuss inverse photoemission in Ce systems and introduce the different types of RIPES measurements. Section III gives a brief description of the RIPES spectrometer. In Sec. IV we present a RIPES study of the α and γ phases of metallic cerium and a collection of experimental results that show the sensitivity of RIPES to T_K in different cerium compounds. The energy dependence of the resonance is more explicitly discussed in Sec. V, while the temperature dependence of the RIPES spectra is described in Sec. VI.

II. RIPES

A. Spectral properties of Ce systems

The minimal theoretical basis for a description of the electronic properties of Ce intermediate valence systems is provided by the celebrated Anderson impurity model (AIM). The model contains $4f$ charge fluctuation and $4f$ conduction-band hybridization energies as parameters. It generates the Kondo scale that controls the low-energy prop-

 © 1997 The American Physical Society

erties and predicts the crossover from localized $4f$ moments at high temperature to a local Fermi liquid with noninteger occupation of the $4f$ states.[14] The AIM, however, explicitly neglects the $4f$ translational degrees of freedom and its validity is based on the generally accepted assumption that coherence effects (considered by more complex and still unsolved lattice models) can safely be neglected except at very low temperatures. According to the AIM, the ground state of a Ce impurity is a hybrid singlet. In the often considered $U_{ff}=\infty$ limit (U_{ff} is the Coulomb repulsion between two $4f$ electrons on the same site), $4f$ occupancies larger than unity are forbidden and the ground state takes the form $|\Psi_G\rangle=a|f^0\rangle+b|f^1\rangle$. This simplified notation indicates that, because of the hybridization between the $4f$ electron and the conduction band, the singlet ground state is an appropriate combination of different $4f$ configurations: $|f^1\rangle$ represents $4f$ electron localized on the Ce ion, while $|f^0\rangle$ indicates the complete transfer of a $4f$ electron to the conduction band. The thermodynamic properties of Ce impurities are determined by the singlet ground state and by a manifold of excited (magnetic) states with pure f^1 character. The energy separation between the singlet and the magnetic states is the Kondo energy k_BT_K and represents the energy gained in the formation of the hybrid ground state. The generalization to finite U_{ff} is conceptually straightforward, although it considerably increases the computational complexity of the problem.

An interpretation of the spectroscopic data based on the AIM has been developed over the past decade, based on numerous experimental results and the comparison with calculational schemes for the spectral properties of the AIM.[15,16] According to this interpretation the vast majority of Ce-based intermediate valence compounds belong to the ''Kondo regime'' of the AIM.[17,18] This ''Kondo paradigm'' has been challenged by more recent results, which have revealed quantitative discrepancies and possible inconsistencies with the predicted spectral properties of the AIM.[19,20] The unsettled controversy raised by the recent data involves fundamental issues as well as complex and poorly explored materials issues (the recent results have been obtained on single crystals, while most of the previous work was on polycrystalline samples) and surface science issues.[21,22] An account of the present status of this debate has been given in Ref. 1. From the theoretical side, alternative schemes or proposed extensions of the AIM are not yet sufficiently developed for a direct comparison with the experimental spectroscopic results.[23,24] Therefore, although the reader should be aware of the existence of alternative viewpoints, throughout this paper we will consistently use the AIM as a guideline for the interpretation of our results.

For the present purposes it is sufficient to recall here some fundamental spectral properties of the AIM.[1,15,16] At $T=0$ the $4f$ electron addition spectrum reflects transitions from the N-electron ground state to all possible final states of the $(N+1)$-electron system, under the effect of a transition operator $a^\dagger$ that creates a $4f$ electron. The extension to $T\neq 0$ will be considered in Sec. VI. The spectrum exhibits two prominent features: a peak centered at energy k_BT_K above E_F (with a spin-orbit satellite separated from the main peak by the $4f$ spin-orbit splitting $\Delta_{so}=0.3$ eV) and a broad structure at energy $\sim\epsilon_f+U_{ff}\sim 4-6$ eV above E_F (ϵ_f is the bare $4f$ energy). The peak near E_F is the so-called Abrikosov-Suhl or Kondo resonance and corresponds to transitions into final states with mainly f^1 ($j=5/2$) character (the satellite has the same orbital symmetry but $j=7/2$ character). The higher-energy structure corresponds to mainly f^2 final states and its width is determined by the energy spread of the f^2 multiplet.[25] Because of the nature of the IPES process, the $|f^0\rangle$ part of the ground state is only coupled to f^1 final states. Therefore, at least in the $U_{ff}=\infty$ limit, the intensity of the ''Kondo resonance'' (KR) reflects the weight of the f^0 configuration in the ground state and the strength of $4f$-band hybridization. More precisely, it can be shown that the intensity of the KR obeys an approximate scaling relation as a function of the parameter T/T_K. This scaling law is one the most fundamental features of the AIM and its experimental verification is an important and controversial issue.[1]

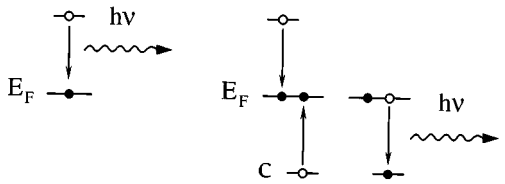

FIG. 1. Schematic description of the interfering direct (left) and indirect (right) transitions of a resonant IPES (RIPES) process.

The broad feature observed near E_F in the experimental IPES spectra is therefore interpreted, in the AIM framework, as a superposition of signal from to the Kondo resonance and its spin-orbit satellite. Due to the finite energy resolution the two features cannot be separated and appear as a unique and broader peak. In the following we shall indifferently refer to the near-E_F peak as the Kondo resonance or the f^1 peak and to the higher-energy feature as the f^2 peak.

B. Resonances in IPES

When the excitation energy crosses the $3d$ or $4d$ ionization thresholds, the Ce $4f$ IPES,[9–12] as well as PES,[2–6] cross sections exhibit resonances due to the quantum interference between transitions involving an intermediate discrete state and a continuum.[26,27] In IPES, the transition to the continuum is the usual or direct process $|\Psi_G(N)\rangle+e^-\rightarrow|\Psi(N+1)\rangle+h\nu$. The discrete state is the intermediate state of an indirect transition $|\Psi_G(N)\rangle+e^-\rightarrow|\Psi^*(N+1),\underline{c}\rangle\rightarrow|\Psi(N+1)\rangle+h\nu$ (Fig. 1), where a core hole ($\underline{c}$) is created and then filled with the emission of a photon. The direct and indirect channels have the same initial and final states and therefore interfere, generating a characteristic resonance profile. In classical terms, the incoming electron drives, via the Coulomb interaction, the resonant oscillation of the $3d$ ($4d$) shell.[28]

The matrix element for the indirect transition contains the overlap between the wave function of the core and of the valence states. Strong resonances may therefore be expected only for rather localized orbitals such as the $3d$ orbitals in the first row of transition metals or the $4f$ orbitals in the lanthanides. The deviation from the normal cross section near threshold depends on the strength of the coupling between the discrete state and the continuum. The orbital sym-

metry of the core and valence orbitals is dictated by dipole selection rules, e.g., d core hole for a $4f$ resonance and p for a d resonance. Resonance spectra therefore contain information on spectral functions (e.g., PES or IPES), projected on a specific site, and on a specific orbital symmetry.

The description of the $4f$ resonance in Ce must take into account the hybrid character of the ground state. The possible direct IPES processes are, schematically,

$$|f^0(G)\rangle + e^- \rightarrow |f^1\rangle + h\nu_1, \tag{1}$$

$$|f^1(G)\rangle + e^- \rightarrow |f^2\rangle + h\nu_2 \tag{2}$$

and the corresponding indirect processes

$$|f^0(G)\rangle + e^- \rightarrow |\underline{c}f^2\rangle \rightarrow |f^1\rangle + h\nu_1, \tag{3}$$

$$|f^1(G)\rangle + e^- \rightarrow |\underline{c}f^3\rangle \rightarrow |f^2\rangle + h\nu_2. \tag{4}$$

Here $|f^0(G)\rangle$ and $|f^1(G)\rangle$ are shorthand notations for the f^0 and f^1 components of the ground state $|\Psi_G\rangle$. On the other hand, 1,3 and 2,4 are not the only radiative channels and one should also consider transitions such as:

$$|f^1(G)\rangle + e^- \rightarrow |\underline{c}f^2k\rangle \rightarrow |f^1k\rangle + h\nu_1^*, \tag{5}$$

where k stands for a spectator conduction electron in the recombination process. This transition corresponds to the characteristic Ce M_α fluorescence observed in x-ray emission spectroscopy (XES) measurements.[29] Unlike the IPES channels (1) and (2), where the photon energies vary with the kinetic energy of the incoming electron, the energy of the M_α emission is fixed. At threshold the M_α signal is degenerate with and indistinguishable from the resonating IPES. This behavior is analogous to that of the Auger lines observed in resonant PES. The XES signal is present even in the atomic limit and its intensity mainly depends on the number of $4f$ holes $n_h = 14 - n_f$. Since n_h is essentially constant for all metallic Ce systems, it can be anticipated that this contribution will show little dependence on the compound, unlike the RIPES itself.

While all the above transitions share the same initial state $|\Psi_G\rangle$, their intermediate and especially final states are largely distinct. The f^1 and the f^2 parts of the IPES spectrum will therefore resonate at different excitation energies. A simple analysis, which does not take multiplet splitting into account, yields the following energy separation: $\Delta E = E(\underline{c}f^3) - E(\underline{c}f^2) = \epsilon_f + 2U_{ff} + U_{fc}$, where U_{fc} represents the $4f$ core hole Coulomb attraction. Typical parameters for Ce systems yield $\Delta E \sim 2$ eV. The relative strength of the f^1 and f^2 resonances should be material dependent and reflect the weight of the f^0 and f^1 configurations in the ground state.

C. RIPES spectra

A typical RIPES measurement is performed by recording a series of IPES spectra at various electron kinetic (i.e., excitation) energies, across the $3d$ threshold. A complete spectrum is recorded for each excitation energy, in contrast with the conventional BIS acquisition mode where a spectrum is collected by scanning the electron energy at a fixed photon energy. Figure 2 illustrates an ideal RIPES measurement.

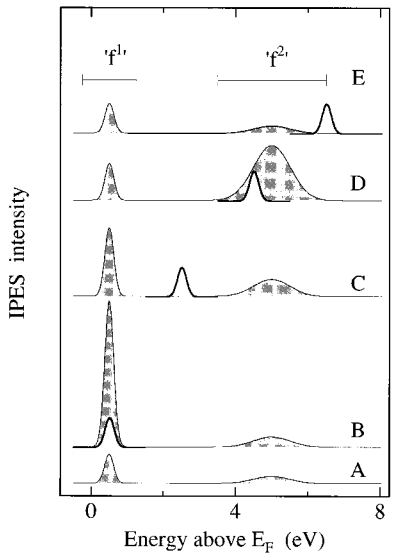

FIG. 2. Schematic view of the results of an ideal Ce $4f$ RIPES experiment. The excitation (electron kinetic) energy increases from A (below threshold) to E (above threshold) and the spectra have been aligned at E_F. The f^1 peak and f^2 manifolds are resonantly enhanced in B and D, respectively. The Ce M_α fluorescence signal (solid line) moves away from E_F with increasing excitation energies. The horizontal bars represent the integration windows for the constant final-state curves of Fig. 4.

The electron energy increases from A (below threshold) to E (above threshold). The initial enhancement of the f^1 peak (B) is followed by the enhancement of the f^2 structure (D). The M_α line, emitted at a constant photon energy, drifts away from E_F as the excitation energy increases. Figure 3 shows the same curves in a different representation, which will be used in the rest of this paper.

It is often difficult to estimate the energy dependence of the resonance from the raw spectra, as in Figs. 2 or 3. A clearer view of the resonance profile is obtained by recording, as a function of electron energy, the integrated intensities of the f^1 and f^2 peaks. Typical integration windows are indicated in Fig. 2 by horizontal bars. Their energy positions track the peak positions as the electron energy is varied. The

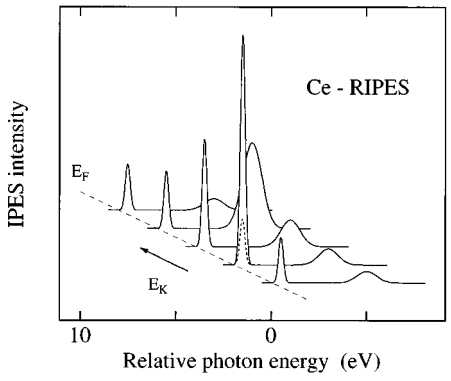

FIG. 3. RIPES spectra of Fig. 2 shown in a different representation. The energy position reflects the actual photon energy. The dashed line represents the position of the Fermi level.

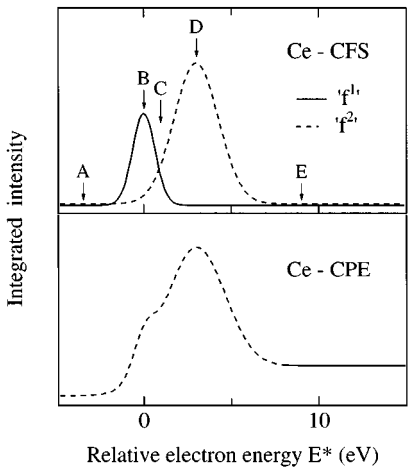

FIG. 4. Top: constant final-state (CFS) curves obtained by integrating, as a function of electron energy, the f^1 and f^2 spectral features of Fig. 2. The letters (A–E) refer to the corresponding RIPES spectra. Bottom: constant photon energy (CPE) curve, obtained by integrating the spectra of Fig. 2 within a fixed energy window centered around the Ce M_α emission. Near threshold (dashed line) the CPE curve is perturbed by overlapping f^1 and f^2 contributions.

resulting constant final-state (CFS) curves are shown in Fig. 4 for the ideal case of Fig. 2. Here and in the following the origin of the relative electron energy (E^*) scale coincides with the maximum of the f^1 curve. The CFS curves directly yield the energy separation and widths of the two resonances and their relative strengths (see below). The related constant photon energy (CPE) measurement is performed by integrating the IPES signal within a fixed window centered at the energy of the M_α line, while varying the electron energy. The structure near threshold is due to the drift of the f^1 and f^2 peaks across the integration window, but well above threshold the CPE curve reflects the M_α intensity and it can be used to estimate the relative importance of the BIS and XES channels near resonance.

Real theoretical calculations of RIPES, as opposed to the qualitative plots of Figs. 2–4, are scarce. Wendin and Nuroh[28] could reproduce the asymmetric IPES resonances observed in La and Ce in Ref. 10 by an atomic calculation that neglected the possibility of mixed valency. The related problem of x-ray emission in Ce materials has been investigated within the AIM,[29] but without considering the threshold excitation of the $4f \rightarrow 3d$ XES. More recently, Tanaka and Jo[30] have performed a realistic calculation of Ce $3d$ RIPES and compared it with the experimental spectra of $CeNi_2$ and $CeRh_3$. They have described the Ce impurity by the Anderson Hamiltonian, with a degenerate conduction band but retaining the full multiplet structure, and treated the resonant transition as an (inverse) second-order coherent optical process. Their results reproduce semiquantitatively the experimental spectra, namely, the distinct enhancement of the f^1 and f^2 features, and the observed energy dependent transfer of spectral weight within the f^2 manifold near threshold (see below). A fully quantitative agreement cannot be achieved because the calculation does not include the incoherent M_α fluorescence process.

III. EXPERIMENTAL DETAILS

The RIPES measurements have been performed on a dedicated UHV spectrometer, which has been described elsewhere.[13] Soft x rays are generated by the interaction of a monochromatic electron beam ($\Delta E = 0.2-0.3$ eV, $I = 0.1-0.2$ mA) with the sample. The kinetic energy of the electrons can be controlled by varying the potential difference (V_0) between the BaO cathode and the sample according to the relation $E_K = eV_0 + \phi_{\rm cath} + 2k_BT \sim eV_0 + 3$ eV, where $\phi_{\rm cath}$ and T are the cathode work function and temperature. The electron beam defines at the sample a 1 mm circular spot, which is also the source of the optical system. The energy analysis of the emitted x rays is performed by a Bragg reflection on a curved beryl $(10\bar{1}0)$ crystal. The dispersed photons are detected by a two-dimensional microchannel plate detector equipped with a resistive anode encoder. The total energy resolution (electrons plus photons) of the apparatus is ~ 0.6 eV.

Polycrystalline samples were prepared by melting stoichiometric amounts of the components in induction furnaces or by a discharge in an Ar atmosphere. The sample quality was checked by x-ray diffraction and, in some cases, by microprobe analysis. The samples were glued with a conducting epoxy on the tip of a He flow cryostat and could be cooled to ~ 15 K. The temperature, measured by a Rh-Fe thermometer in close thermal contact with the sample, could also be regulated to better than 1 K over the whole 300–15 K range by a resistive heater. Fresh surfaces were prepared *in situ* by scraping with a diamond file at a base pressure of 1×10^{-10} torr. Thin films of the α and γ phase of Ce were prepared as usual by evaporating high purity Ce from a tungsten filament onto a Cu substrate kept, respectively, at 20 and 300 K.

IV. RESULTS AND DISCUSSION

A. Metallic cerium

The α-γ transition in metallic cerium[31] is an inescapable test of any spectroscopic probe of mixed valence. Spectroscopic data[32,33] have played a major role in establishing the ''Kondo volume collapse'' (KVC) model of the transition, based on the AIM.[34,35] According to the KVC, the two phases represent two different regimes of the Kondo behavior: $T > T_K$ in the γ phase ($T_{K\gamma} \sim 100$ K) and $T \ll T_K$ ($T_{K\alpha} \sim 1000$ K) in the α phase. Such a large difference has important consequences on the spectroscopic properties. In the combined high-resolution PES/BIS spectra of Fig. 5 the Kondo resonance is much stronger in the α phase, as predicted by the AIM. The difference is especially clear in the BIS part, which confirms that despite its limited resolution (the KR and its satellite cannot be separated) inverse photoemission is an extremely powerful probe of Ce systems.

The different spectral properties of α- and γ-Ce are also manifest in the RIPES results. For both phases the CFS curves of Fig. 6 exhibit clear maxima, separated by ~ 1 eV, but the f^1 curve is much weaker in γ-Ce. The ratio R of the two maxima is ~ 0.2 for γ-Ce and ~ 0.5 for α-Ce (Table I). The intensities of the CFS curves are partially affected by the nonresonating Ce M_α signal. This contribution can be roughly estimated by comparing the CFS and CPE curves.

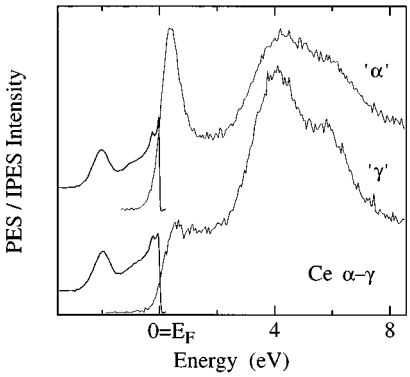

FIG. 5. Combined PES ($h\nu$=48.4 eV, thick lines) and BIS ($h\nu$=1486 eV, thin lines) spectra of α-Ce and γ-Ce.

The width of the integration window for the CPE and the f^1 CFS measurements were the same, so that the intensities are strictly comparable. Close to threshold the CPE curve is distorted by the overlapping contribution of the f^1 and f^2 features, but above $\sim$10 eV the curve is smooth, with a positive slope reflecting an increasing density of final states. The extrapolation of the slope towards threshold (dashed lines) suggests that approximately one-half of the f^1 CFS signal in γ-Ce, and $\sim$25% in α-Ce, is due to incoherent emission.

The RIPES spectra of α- and γ-Ce, measured at the maximum of the f^1 resonance profile, are shown in Fig. 7. As for the conventional BIS spectra, the KR is predominant in α-Ce, while the f^2 peak is larger in γ-Ce, even at this energy. The obvious advantage of RIPES is the much larger (1–2 orders of magnitude) intensity, which considerably reduces the acquisition time and the risk of surface contamination. A comparison of the BIS and RIPES results shows that in RIPES the characteristic sloping background is much weaker. A second difference is the reduced width of the f^2 feature in the RIPES spectra. Both are consequences of the

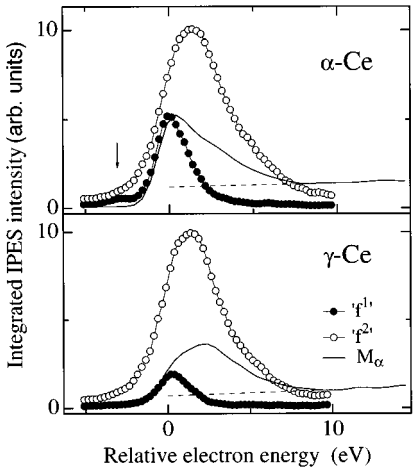

FIG. 6. RIPES CFS (f^1, solid symbols; f^2, empty symbols) and CPE curves of α-Ce and γ-Ce. A linear extrapolation of the CPE curve is used to estimate the contribution at threshold of the fluorescence signal. The arrow marks a prethreshold feature, discussed in Sec. V.

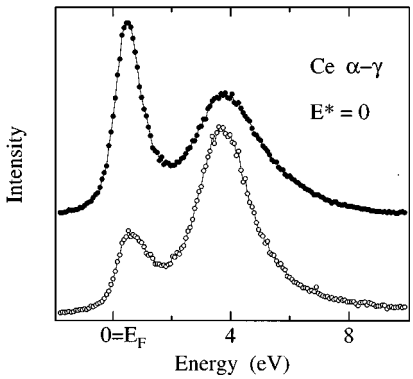

FIG. 7. RIPES spectra of α-Ce (solid symbols) and γ-Ce (empty symbols) measured at the maximum of the f^1 resonance.

RIPES selection rules and of the nonuniform enhancement of the various terms of the f^2 multiplet.[30]

We looked for possible figerprints of the α-γ phase transition, but our measurements revealed only very small and continuous spectral changes when the temperature of the evaporated film was varied between room temperature (RT) and 20 K (or vice versa) over a period of about 1 h. We conclude that, at least near the surface, the evaporated thin films did not undergo the α-γ transition, possibly because of the well-known perturbing effect of the hcp β-Ce phase.[31]

B. Overview of the RIPES results

In this section we present an overview of experimental RIPES data for various cerium-based materials. For the sake of clarity we have grouped these results in three subsections: weakly hybridized materials, typical Kondo systems, and strongly hybridized materials. It is, however, clear that this division is somewhat arbitrary and that the boundaries between the different representative classes are not sharp.

1. Weakly hybridized Ce compounds

We consider in this section three representative low-T_K compounds, with magnetic ground states CeSb, $CeGe_2$, and Ce_7Rh_3. CeSb, which crystallizes in the cubic NaCl structure, orders below T_N=17 K with a large Ce moment of 1.9 μ_B and exhibits a complex phase diagram.[36] Valence-band x-ray photoemission spectroscopy (XPS) and BIS data reveal a semimetallic character, with a very small density of states at the Fermi level.[37,38] The 3d core level spectra are also indicative of nearly localized 4f electrons, but coherence effects are believed to be important.[39] Orthorhombic $CeGe_2$ exhibits a Curie-Weiss behavior with effective moments equal to 95% of the Ce^{3+} value and orders ferromagnetically below 7 K. Specific-heat measurements suggest a residual Kondo effect with $T_K\sim$2 K.[40] Ce_7Rh_3, which crystallizes in the Th_7Ni_3 structure with Ce ions in three inequivalent sites, exhibits a magnetic transition at 7 K and some evidence for Kondo behavior on one of the sublattices.[41] Core-level and valence-band PES, as well as BIS (Ref. 42) data, are consistent with a weak hybridization.

The weakly hybridized character of these compounds is confirmed by the high-resolution PES spectra of Fig. 8. According to the AIM, the Ce 4f spectral function exhibits two

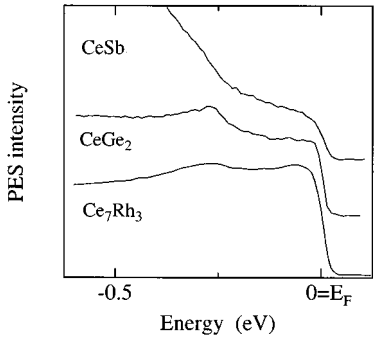

FIG. 8. High-resolution PES spectra ($h\nu = 40.8$ eV) of three weakly hybridized Ce compounds. The peak at -0.3 represents a $4f$ spin-orbit excited state.

sharp features in this energy range: the tail of the KR, cut by the Fermi distribution function, and a spin orbit satellite at -0.3 eV. The two features are unequally sensitive to the $4f$-band hybridization strength, the KR being the more sensitive, and the ratio of their intensities can be used to estimate the value of T_K.[43] The small intensity of the KR in the spectra of Fig. 8 sets un upper limit $T_K \sim 10$–30 K for the three compounds. The hybridization appears to be largest in Ce_7Rh_3, where the tail of the KR is as intense as the spin-orbit satellite, and smallest in CeSb. The spectrum of CeSb, which is strongly dominated by the emission from the Sb sp states, steeply rising away from E_F, is really unique among Ce compounds for the total absence of $4f$-related features.

The RIPES spectra of Fig. 9 are dominated by the resonating f^2 structures. In CeSb the f^2 peak is strongest and apparently sharpest and the emission in the vicinity of the Fermi level is vanishingly small at all excitation energies, although there are signs of the M_α line drifting away from E_F. The intensity in the f^1 region is larger in Ce_7Rh_3 and the f^2 structure is broadened by the fluorescence signal. Only in $CeGe_2$ is it possible to identify a resonating f^1 peak. These observations are confirmed by the CFS curves. CeSb has the smallest R ratio (0.10), only one-half the value of γ-Ce (Table I), so that the apparent weak f^1 resonance should probably be entirely attributed to fluorescence. R is largest in $CeGe_2$ and, perhaps surprisingly, slightly larger than in γ-Ce. Some caution is, however, appropriate here, since the resonating signal from possible parasitic phases (oxides, etc.) could perturb the quantitative determination of the resonance profile. Our samples presented very small

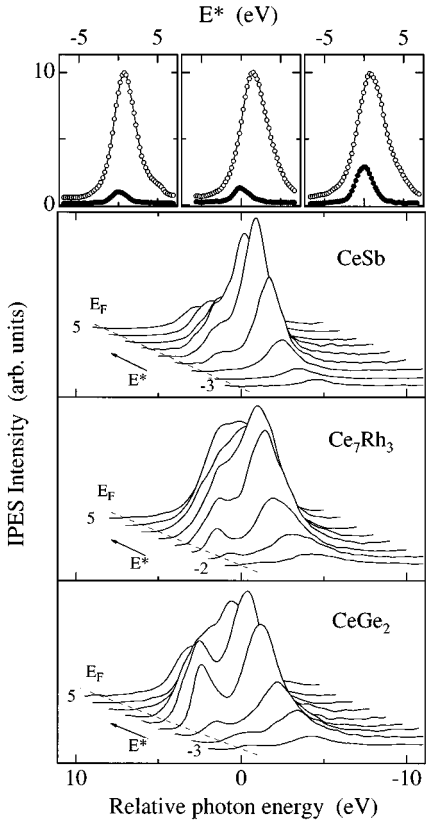

FIG. 9. RIPES spectra of CeSb, Ce_7Rh_3, and $CeGe_2$. The top panels show the corresponding CFS curves: CeSb (left), Ce_7Rh_3 (middle), and $CeGe_2$ (right). The resonance profiles are dominated by the f^2 structures (open symbols).

amounts of parasitic phases, and clean surfaces were prepared in good vacuum by a standard procedure. Moreover, we observed little evidence of evolution of the spectra during the acquisition time. However, our present apparatus does not allow us to check possible contamination with independent surface sensitive probes. Although we are convinced that our results represent intrinsic properties, this limitation should be addressed by future experiments.

2. Typical Kondo systems

In this section we consider three representative Kondo systems $CeSi_2$, $CePd_3$, and $CeNi_2$. The hybridization in these materials is stronger than in the compounds considered in Sec. IV B 1 and the estimated T_K values are correspond-

TABLE I. Experimental values of the ratio (R) between the maximum integrated intensities of the f^1 and f^2 RIPES constant final state curves, in various cerium-based materials.

Material	$R = \max(f^1)/\max(f^2)$	Material	$R = \max(f^1)/\max(f^2)$
CeSb	0.10	α-Ce	0.52
Ce_7Rh_3	0.13	$CePd_7$	0.63
γ-Ce	0.20	$CeFe_2$	1.15
$CeSi_2$ (300 K)	0.27	$CeNi_2$	1.37
$CeGe_2$	0.29	$CeRh_2$	3.0
$CePd_3$ (300 K)	0.43	$CeRh_3$	4.8
$CePd_3$ (50 K)	0.55		

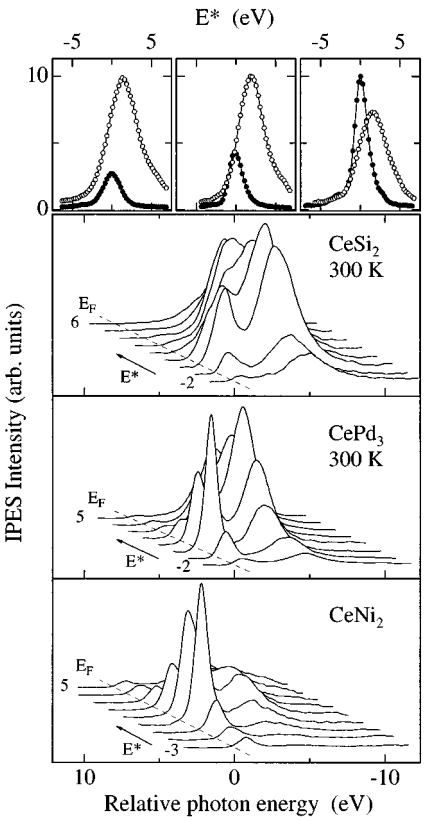

FIG. 10. RIPES spectra of CeSi2, $CePd_3$, and $CeNi_2$. The top panels show the corresponding CFS curves: CeSi2 (left), $CePd_3$ (middle), and $CeNi_2$ (right). The intensity of the f^1 resonance increases with the strength of the $4f$-band hybridization.

ingly larger, in the range $\sim 100-1000$ K. $CeSi_2$ is nonmagnetic and its Kondo temperature has been estimated by different techniques at 50–100 K.[44,45] $CePd_3$ is a much studied Kondo material. Quasielastic neutron scattering data yield $T_K \sim 240$ K,[46,47] while magnetic susceptibility and NMR measurements suggest slightly larger values (~ 350 K).[48] Both the $3d$ XPS and the $2p$ x-ray absorption spectroscopy (XAS) spectra exhibit satellites that indicate a sizable configuration mixing.[49,50] For $CeNi_2$ spectroscopic data indicate an even larger hybridization and effective valence, at the limit of the Kondo regime, with $T_K > 1000$ K.

The RIPES spectra of $CeSi_2$, $CePd_3$, and $CeNi_2$ are shown in Fig. 10. For $CeSi_2$ and $CePd_3$, where T_K falls within the experimentally attainable temperature range, we observe (Sec. VI) measurable changes between 20 K ($T < T_K$) and RT ($T > T_K$). The RT spectra of $CeSi_2$ are similar to those of $CeGe_2$, with a predominant f^2 structure at all excitation energies, but a clearly visible f^1 peak at resonance. The R value (0.27) is also close to that of $CeGe_2$. The RIPES spectra of $CePd_3$ present a separate enhancement of the f^1 and f^2 structures and a much larger R ratio (0.43). The RIPES spectrum measured at the top of the f^1 resonance profile ($E^*=0$) is compared in Fig. 11 with the conventional BIS spectrum of $CePd_3$. The absence of the ''split-off d-band'' peak at ~ 2.2 eV (Ref. 51) in the RIPES spectrum illustrates the orbital selectivity of the resonance process. The $E^*=3$ eV spectrum shows a strong spectral weight transfer from the KR to the higher-energy part of the f^2 multiplet and yet no intermediate peak. The RIPES spectra of $CeNi_2$ are dominated by the KR and the value of the R ratio is 1.37, the largest of the materials considered so far. A similar value ($R=1.2$) was observed in $CeFe_2$ (not shown), a material with a formal valence close to that of $CeNi_2$.

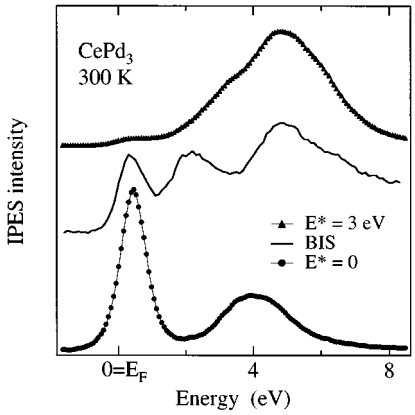

FIG. 11. RIPES spectra of $CePd_3$ measured at the maximum of the f^1 (bottom) and f^2 (top) resonance, compared with the conventional BIS spectrum. One should notice the transfer of spectral weight from the f^1 peak to the f^1 manifold and the absence of the intermediate split-off d state in the RIPES spectra.

The results of this section show that the relative strengths of the f^1 and f^2 resonances increases with the strength of the f-band hybridization. This increase reflects the larger weight of the f^0 configuration in the hybrid ground state. The resonance profiles of Fig. 10 can therefore be exploited, together with other spectroscopic data, to determine the strength of configuration mixing in the ground state. From the experimental point of view, RIPES offers over conventional BIS the advantage of a large and selective amplification of the $4f$ signal, as shown explicitly by the example of $CePd_3$.

3. Strongly hybridized materials: The intermediate valence limit

We review in this section the RIPES results for $CeRh_2$, $CeRh_3$, and $CePd_7$, three strongly hybridized intermetallic compounds close to the intermediate valence regime, at the borderline of validity of the Kondo model. Valence-band and core-level XPS and $L_{2,3}$ XAS spectra indicate a strong valence mixing[7,52–54] and the IPES spectra are characterized by a very intense Kondo resonance, unusually far (~ 1 eV) from E_F.[8] Their physical properties indicate a clear tendency towards the delocalization of the $4f$ states.[55,56] This tendency is particularly strong in $CeRh_3$ and in $CePd_7$, where the measured values of the static magnetic susceptibility and of the linear coefficient of the specific heat are close to free-electron values. The properties of $CeRh_2$, on the other hand, are closer to those of $CeNi_2$. Recent local-density calculations,[57] with the apparent support of spectroscopic data on $CeRh_3$,[58] suggest that a band approach could provide an appropriate description of the $4f$ states in such strongly hybridized materials. At the present time, however, this issue is far from being settled.

The RIPES spectra $CeRh_3$ and $CeRh_2$ of Fig. 12 are dominated, like the conventional BIS spectra, by the f^1 peak. At resonance the intensity of this feature is quite large and a

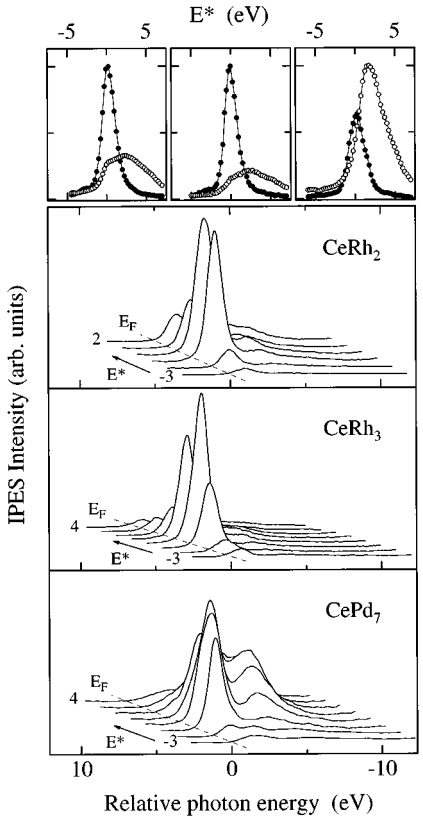

FIG. 12. RIPES spectra of $CeRh_2$, $CeRh_3$, and $CePd_7$. The top panels show the corresponding CFS curves: $CeRh_2$ (left), $CeRh_3$ (middle), and $CePd_7$ (right). The f^1 structure dominates the resonance profiles of $CeRh_2$ and $CeRh_3$, but, surprisingly, not that of $CePd_7$.

spectrum can be collected with acceptable statistics in few minutes, as opposed to the several hours necessary to record a BIS spectrum. The f^2 manifold is extremely weak in $CeRh_3$ and it is probably mostly associated with a surface contribution,[8] while it is more pronounced in the spectra of $CeRh_2$. The R ratios, 3 for $CeRh_2$ and 4.8 for $CeRh_3$, are by far the largest we have observed and are consistent with the very large configuration mixing in the ground state of these materials. These values are somewhat perturbed by the M_α fluorescence signal, which accounts for a large portion of the measured integrated f^2 intensity, a situation opposite that of the weakly hybridized CeSb or Ce_7Rh_3.

The examples considered in this and in the previous sections demonstrate a correspondence between the Kondo temperatures and the strengths of the resonances in RIPES. Increased $4f$-band hybridization and T_K seem to lead invariably to the enhancement of the f^1/f^2 ratio. $CePd_7$, however, does not fit in this systematic trend. The RIPES spectra exhibit a sizable f^2 peak and the R value (0.63) is much smaller than in $CeRh_3$. Further combined PES/RIPES measurements will be necessary to clarify this surprising result.

V. THE RESONANCE PROFILE AND THE ENERGY DEPENDENCE OF THE SPECTRAL LINE SHAPE

The results of the previous sections demonstrate that not only the intensity but also the spectral line shape of the Ce IPES spectra strongly depend on the excitation energy near the Ce M_5 edge. Two different but related effects can produce such energy-dependent changes: the configuration dependence of the resonance profile and the rapidly changing ratio of the cross section for the $4f$ and band states. The first effect has already been mentioned in Sec. II. IPES transitions involving different ionic configurations (f^0, f^1) resonate at different excitation energies, as implied by Eqs. (3) and (4). Since final states with predominantly f^1 or f^2 character are well separated in energy, different parts of the IPES spectrum are sequentially enhanced as a function of the excitation energy. The shape of the resonance profiles is determined by the energy distribution of the complex $3d^9 4f^2$ and $3d^9 4f^3$ intermediate-state multiplets and by selection rules. The electron-induced excitation processes do not impose strict conditions on the angular momenta (the matrix elements are transition elements for an inverse Auger process). On the other hand, the deexcitation processes must obey dipole selection rules, so that only a subset of the intermediate multiplet is coupled to final states. The problem is strictly related to that of $3d$ x-ray absorption,[59] but because of the extra electron in RIPES, the f^1 and f^2 CFS profiles should be compared, respectively, with the XAS spectra of Ce^{3+} (f^1) and Pr^{3+} (f^2). The individual, broadened, multiplet states are too closely spaced to be resolved in the CFS curve, but it is interesting to notice that the small prepeak, clearly visible in some of the f^1 resonance profiles ~ 3 eV below the maximum (e.g., in Fig. 6), is also observed in the $3d$ absorption spectra of the early rare-earth elements.

The rapid relative cross-section changes near the $4d$ or $3d$ thresholds are well known in PES and have been exploited in studies of Ce materials to extract the Ce $4f$ contribution through the comparison of on- and off-resonance spectra. Both the PES and IPES (Ref. 12) $4d \rightarrow 4f$ resonances in the rare-earth elements exhibit asymmetric Fano profiles, with a minimum of the cross section before the edge, so that the $4f$ emission can be not only enhanced, but also depressed with respect to the signal from band states. The situation is less clear at the $3d$ edge, where the resonance profile is dominated by a complex multiplet structure. Our prethreshold measurements indicate a strong depression of the $4f$ IPES cross section in $CeRh_3$ and $CePd_3$. Figure 13 shows the RIPES spectra of $CeRh_3$ for excitation energies below threshold. The $E^* = -4$ eV spectrum is similar to the conventional BIS spectrum, with a prominent f^1 peak and a much weaker feature around 4 eV. At lower excitation energies the intensity of the f^1 peak rapidly decreases. This produces a rather spectacular change of the spectral line shape in just few eV and the prominent feature of the $E^* = -9$ eV spectrum is the 4-eV peak. A comparison with the calculated partial densities of states from Ref. 57 shows that this spectrum reflects the unoccupied d band.[60] The prethreshold spectra of $CePd_3$ of Fig. 14 present a similar evolution. The $4f$ peaks are progressively depressed at lower energy and disappear at $E^* = -8$ eV, while an intermediate structure (the split-off d band) emerges at ~ -2 eV. Therefore the character of the RIPES spectrum rapidly changes from $4f$ sensitive to d sensitive below the $3d$ threshold. A suppression of the $4f$ IPES intensity could also be achieved by working at much lower energy, in the UV range ($h\nu < 15$

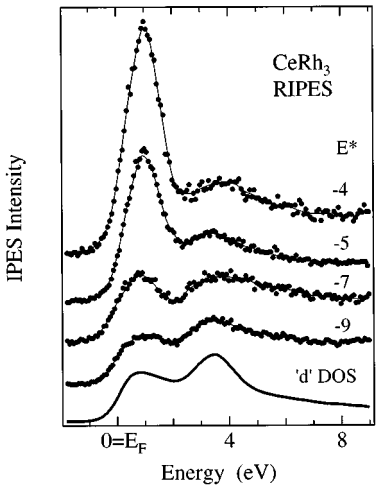

FIG. 13. Line shape of the prethreshold RIPES spectra of $CeRh_3$, suggesting a transition from f sensitive ($E^*=-4$ eV) to d sensitive ($E^*=-9$ eV). The solid line is the d partial density of states from Ref. 52.

eV), but only at the expense of a much larger surface sensitivity.[8]

VI. TEMPERATURE DEPENDENCE OF THE 4f SIGNAL

As discussed in the Introduction, the properties of Kondo systems reveal a characteristic, hybridization-dependent, low-energy scale k_BT_K. According to the AIM, most physical quantities obey simple approximate scaling laws with the single parameter T/T_K.[16] The $4f$ spectral function are expected to exhibit a similar scaling behavior. The model predicts that, as temperature is increased from 0 to $T \gg T_K$, the intensity of the Kondo resonance is reduced and spectral weight is transferred to the f^2 peak.[16,61] This peculiar temperature dependence should manifest itself in the IPES spectra of Ce and, because of the electron-hole symmetry of the AIM, also in the PES spectra of the Yb compounds (the KR is mostly occupied in Yb). Attempts to test this crucial prediction of the model by PES in Yb-based materials have

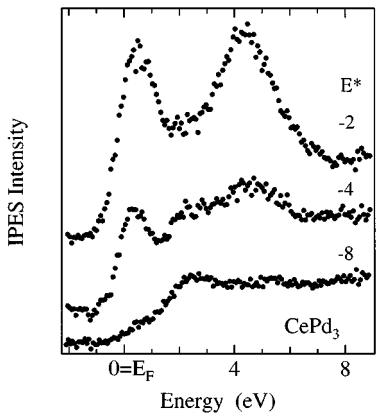

FIG. 14. Prethreshold RIPES spectra of $CePd_3$. At $E^*=-8$ eV the $4f$ signal is strongly depressed and the main spectral feature is the split-off d state.

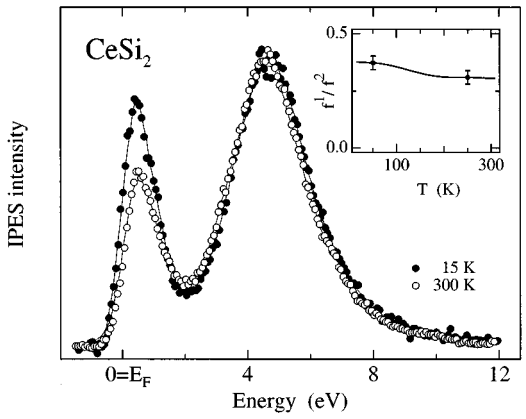

FIG. 15. RIPES spectra of $CeSi_2$ measured at the maximum of the f^1 resonance at 15 K (solid symbols) and at RT, and normalized at the top of the f^2 structure. The intensity variation of the Kondo peak is qualitatively consistent with the predictions of the AIM. Inset: Temperature dependence of the experimentally determined f^1/f^2 intensity ratio, with typical error bars.

yielded contrasting results,[62–64] possibly because of the peculiar sensitivity of the Yb $4f$ configuration to surface conditions. Inverse photoemission, which is less surface sensitive than PES, is well suited to investigate the expected spectral changes in Ce systems. Even the poor experimental resolution is not an obstacle in this case because the interesting quantity is the integrated spectral weight of the KR and its spin-orbit satellite. Recent BIS studies of $CePd_3$ and $CeSi_2$ have indeed revealed temperature-dependent changes that are qualitatively consistent with the predictions of the AIM.[65,66]

Thanks to the short acquisition time of a RIPES spectrum (a few minutes) we could collect data on the same surface at several different temperatures and even continuously follow the temperature dependence of the spectra. Figure 15 shows the temperature dependence of the RIPES spectra of $CeSi_2$ ($T_K=50-100$ K). The spectra, collected at 15 and 300 K at the maximum of the f^1 resonance ($E^*=0$), have been (arbitrarily) normalized at the top of the f^2 peak. This procedure masks the transfer of spectral weight from the low- to the high-energy structure, but it is probably appropriate in this particular case because, due to the choice of the excitation energy, any relative variation of the f^2 weight is strongly reduced. A comparison of the two spectra confirms the expected growth of the f^1 peak at low temperature, with a 25% increase at 15 K. This figure should be compared with the $\sim$ 15% increase observed by conventional BIS, when the spectra are normalized in the same way.[66] Of course one should not expect an identical result in the two cases since the spectra reflect partially different quantities. In conventional BIS the f^1 peak contains a contribution from conduction-band states, which is difficult to estimate, and from the inelastic background. The RIPES spectra single out the emission from the Ce $4f$ states, but at resonance the leading peak has an underlying Ce M_α contribution. A quantitative evaluation of this contribution is beyond the scope of the present paper and our main purpose is to establish qualitatively the temperature effect. From the experimental point of view, the large overall intensity gain represents a clear

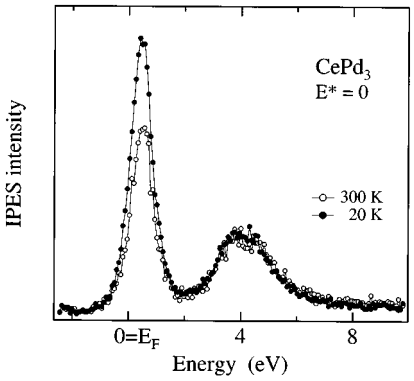

FIG. 16. RIPES spectra of $CePd_3$ (at $E^*=0$, and normalized at the top of the f^2 structure) showing a strong variation of the Kondo peak intensity between 20 and 300 K.

advantage of RIPES over conventional BIS and allows us to exclude trivial artifacts of the measurement.

We have recorded the integrated f^1 and f^2 intensities in $CeSi_2$ throughout the temperature range 15 K to RT. Both signals slightly decreased during the 1-h scans, suggesting the absorption of some residual gas. In order to compensate this spurious intensity variation, we plot in the inset of Fig. 15 the f^1/f^2 ratio. The solid line is a smooth fit to the experimental data (measured every ~ 5 K), obtained by summing several separate scans, each performed on a fresh surface prepared at 300 K. The ratio clearly increases at low temperature and the curve even suggests the existence of the expected plateaus well above and well below T_K, as expected from the temperature dependence of the Kondo resonance, even if the statistical error bars are still too large for a quantitative analysis. Moreover, no detailed theoretical predictions are available for the temperature dependence of the spectral function at resonance and the results of Ref. 16 should be considered only as a qualitative guideline.

The low-temperature increase of the Kondo peak is confirmed by the $CePd_3$ data of Fig. 16. The spectra have been measured at the f^1 resonance, on the same surface prepared at 300 K and then cooled. The growth of the KR at the lower temperature cannot be due to surface contamination because a prolonged exposure to the residual vacuum always produced a relative decrease of the f^1 peak. We have repeated the measurement on many surfaces prepared at 300 K and at 20 K. The results are very reproducible and show that the integrated f^1/f^2 intensity ratio (at $E^*=0$) changes from 1.25 ± 0.02 at 300 K to 1.69 ± 0.02 at 20 K. We have also observed that the R ratio increases from 0.43 at 300 to 0.55 at 50 K. We have not observed, on the other hand, any temperature dependence between 300 K and 20 K in the RIPES spectra of $CeRh_3$. This result is perfectly consistent with the Kondo model and with the fact that the estimated Kondo temperature of $CeRh_3$ lies well above the explored temperature range.

The previous results demonstrate the unconventional temperature dependence of the IPES spectral function of Ce-based materials. The observed changes are consistent with the predictions of the Kondo model, which interprets them as an identifying characteristic of the crossover from the high-temperature ($T \gg T_K$) local moment regime to the low-temperature ($T \ll T_K$) Fermi-liquid behavior.

VII. CONCLUSION

We have exploited a spectroscopic technique, resonant inverse photoemission, to investigate the electronic structure of various Ce-based materials, spanning a wide range of physical properties and Kondo temperatures. In all cases the overall intensity of the inverse photoemission spectrum is resonantly enhanced when the excitation energy equals the Ce $3d$ absorption threshold. At resonance the spectrum reflects only the Ce $4f$ contribution. A closer analysis shows that the f^1 (Kondo resonance) and f^2 spectral features have distinct resonance profiles. The systematic investigation of different materials strongly suggests that the relative intensity of the f^1 and f^2 resonance profiles is directly related to the $4f$-band hybridization strength in the ground state. By exploiting the large intensity gain at the resonance we have been able to probe, with improved accuracy over conventional measurements, the temperature dependence of the IPES spectral function. The RIPES results unambiguously establish that the intensity of the Kondo peak increases when the temperature is decreased below T_K.

Resonant inverse photoemission is an interesting probe of the electronic structure of cerium-based materials, with valuable advantages over conventional IPES. The sensitivity to the Ce $4f$ states can be varied by 2–3 orders of magnitude by a small change of the electron energy. Combined on- and off-resonance data can therefore be exploited to study the character (local vs extended) of the electronic states in Ce compounds, under otherwise identical experimental conditions. These improvements have a direct impact on the quality of the experimental results and open the way to more sophisticated experiments, namely, to crucial experiments on single-crystal surfaces.

ACKNOWLEDGMENTS

This work has been supported by the Swiss National Science Foundation. We are grateful to Professor G.L. Olcese, Dr. E. Beaurepaire, and G. Schmerber for lending us some of the Ce samples. We acknowledge stimulating discussions and correspondence with L. Braicovich, H. Eskes, and T. Jo. The assistance of L. Leuwen was highly appreciated.

*Present address: Institut de Physique Appliquée, Ecole Polytechnique Fédérale, CH-1015 Lausanne, Switzerland.

†Present address: Nanoscale Physics Research Laboratory, University of Birmingham, Birmingham B15 2TT, United Kingdom.

‡Present address: Laboratoire de Physique du Solide, Université H. Poincaré, Boîte Postale 239, F-54506 Vandœuvre les Nancy, France.

[1] For a recent review see D. Malterre, M. Grioni, and Y. Baer, Adv. Phys. **45**, 299 (1996).

[2] W. Lenth, F. Lutz, J. Barth, G. Kalkoffen, and C. Kunz, Phys. Rev. Lett. **41**, 1185 (1978).

[3] J.W. Allen, L.I. Johansson, R.S. Bauer, I. Lindau, and S.B.M. Hagström, Phys. Rev. Lett. **41**, 1499 (1978).

[4] G. Kaindl, G. Kalkowski, W.D. Brewer, B. Perscheid, and F.

Holtzberg, J. Appl. Phys. **55**, 1910 (1984).
[5] J.W. Allen, S.-J. Oh, I. Lindau, and L.I. Johansson, Phys. Rev. B **29**, 5927 (1984).
[6] C. Laubschat, E. Weschke, G. Kalkowski, and G. Kaindl, Phys. Scr. **41**, 124 (1990).
[7] G. Chiaia, P. Vavassori, L. Duò, L. Braicovich, M. Qvarford, and I. Lindau, Surf. Sci. **331-333**, 1229 (1995).
[8] L. Braicovich, L. Duò, P. Vavassori, D. Malterre, M. Grioni, Y. Baer, and G.L. Olcese, Physica B **206&207**, 77 (1995).
[9] P. Weibel, M. Grioni, D. Malterre, B. Dardel, and Y. Baer, Phys. Rev. Lett. **72**, 1252 (1994).
[10] R.J. Liefeld, A.F. Burr, and M.B. Chamberlain, Phys. Rev. A **9**, 316 (1974); M.B. Chamberlain, A.F. Burr, and R.J. Liefeld, *ibid.* **9**, 663 (1974).
[11] F. Riehle, Ph.D. thesis, Karlsruhe Universität, 1977; Jpn. J. Appl. Phys. Suppl. **17**, 314 (1978).
[12] A.S. Shulakov, T.M. Zimkina, and V.A. Formichev, Izv. Akad. Nauk SSSR **49**, 1495 (1985).
[13] P. Weibel, M. Grioni, C. Hêche, and Y. Baer, Rev. Sci. Instrum. **66**, 3755 (1995).
[14] A.C. Hewson, *The Kondo Problem to Heavy Fermions* (Cambridge University Press, Cambridge, 1993), and references therein.
[15] O. Gunnarsson and K. Schönhammer, Phys. Rev. B **28**, 4315 (1983).
[16] N.E. Bickers, D.L. Cox, and J.W. Wilkins, Phys. Rev. B **36**, 2036 (1987).
[17] J.W. Allen, S.-J. Oh, O. Gunnarsson, K. Schönhammer, M.B. Maple, M.S. Torikachvili, and I. Lindau, Adv. Phys. **35**, 275 (1986).
[18] F. Patthey, J.M. Imer, W.-D. Schneider, H. Beck, Y. Baer, and B. Delley, Phys. Rev. B **42**, 8864 (1990).
[19] J.J. Joyce *et al.*, Phys. Rev. Lett. **68**, 236 (1992); Physica B **186-188**, 31 (1993).
[20] A.B. Andrews *et al.*, Phys. Rev. B **51**, 3277 (1995); **53**, 3317 (1996).
[21] C. Laubschat, E. Weschke, C. Holtz, M. Domke, O. Strebel, and G. Kaindl, Phys. Rev. Lett. **65**, 1639 (1990).
[22] L. Duò, P. Vavassori, L. Braicovich, M. Grioni, D. Malterre, Y. Baer, and G.L. Olcese, Phys. Rev. B **53**, 7030 (1996).
[23] Q.G. Sheng and B.R. Cooper, Philos. Mag. Lett. **72**, 123 (1995).
[24] A.N. Tahlvidar-Zadeh, M. Jarrel, and J.K. Freericks (unpublished).
[25] J.K. Lang, Y. Baer, and P.A. Cox, J. Phys. F **11**, 121 (1981).
[26] U. Fano, Phys. Rev. **124**, 1866 (1961).
[27] L.C. Davis and L.A. Feldkamp, Phys. Rev. A **17**, 2012 (1978).
[28] G. Wendin and K. Nuroh, Phys. Rev. Lett. **39**, 48 (1977).
[29] S. Tanaka, H. Ogasawara, Y. Kayanuma, and A. Kotani, J. Phys. Soc. Jpn. **58**, 1087 (1989); S. Tanaka, Y. Kayanuma, and A. Kotani, *ibid.* **58**, 4626 (1989).
[30] A. Tanaka and T. Jo, Physica B **206&207**, 74 (1995); J. Phys. Soc. Jpn. **65**, 615 (1996).
[31] D.C. Koskenmaki and K.A. Gschneidner, in *Handbook on the Physics and Chemistry of the Rare Earths*, edited by K.A. Gschneidner and L. Eyring (North-Holland, Amsterdam, 1978), Chap. 4.
[32] E. Wuilloud, H.R. Moser, W.-D. Schneider, and Y. Baer, Phys. Rev. B **28**, 7354 (1983).
[33] L.Z. Liu, J.W. Allen, O. Gunnarsson, N.E. Christensen, and O.K. Andersen, Phys. Rev. B **45**, 8934 (1992).
[34] J.W. Allen and R.M. Martin, Phys. Rev. Lett. **49**, 1106 (1982).
[35] J.W. Allen and L.Z. Liu, Phys. Rev. B **46**, 5047 (1992).
[36] J. Rossat-Mignod, P. Burlet, S. Quezel, and O. Vogt, Physica **102B**, 237 (1980).
[37] Y. Baer, R. Hauger, Ch. Zürcher, M. Campagna, and G.K. Wertheim, Phys. Rev. B **18**, 4433 (1978).
[38] F.U. Hillebrecht, W. Gudat, N. Mårtensson, D.D. Sarma, and M. Campagna, J. Magn. Magn. Mater. **47&48**, 221 (1985).
[39] H. Kitazawa, I. Oguro, M. Hirai, Y. Kondo, T. Suzuki, and T. Kasuya, J. Magn. Magn. Mater. **47&48**, 532 (1985).
[40] H. Yashima, T. Satoh, H. Mori, D. Watanabe, and T. Ohtsuka, Solid State Commun. **41**, 1 (1983); H. Mori, H. Yashima, and N. Sato, J. Low Temp. Phys. **58**, 513 (1985).
[41] J.G. Sereni, O. Trovarelli, G. Schmerber, and J.P. Kappler, J. Magn. Magn. Mater. **108**, 183 (1992).
[42] P. Vavassori, L. Duò, L. Braicovich, and G.L. Olcese, Phys. Rev. B **50**, 9561 (1994); L. Duò, P. Vavassori, L. Braicovich, M. Grioni, D. Malterre, Y. Baer, and G.L. Olcese, *ibid.* **53**, 7030 (1996).
[43] D. Malterre, M. Grioni, P. Weibel, B. Dardel, and Y. Baer, Phys. Rev. B **48**, 10 599 (1993).
[44] H. Yashima, H. Mori, T. Satoh, and K. Kohn, Solid State Commun. **43**, 193 (1982).
[45] R.M. Galera, A.P. Murani, and J. Pierre, Physica B **156&157**, 801 (1989).
[46] S.M. Shapiro, C. Stassis, and G. Aeppli, Phys. Rev. Lett. **62**, 94 (1989).
[47] More recent neutron data [A.P. Murani, R. Raphel, Z.A. Bowden, and R.S. Eccleston, Phys. Rev. B **53**, 8188 (1996)], however, suggest a much larger $T_K \sim 600$ K.
[48] A. Qachaou, E. Beaurepaire, M. Benakki, B. Lemius, J.P. Kappler, A.J.P. Meyer, and P. Panissod, J. Magn. Magn. Mater. **63&64**, 635 (1987).
[49] G. Krill, J.P. Kappler, A. Meyer, L. Abadli, and M.F. Ravet, J. Phys. F **11**, 1713 (1981).
[50] J.C. Fuggle, F.U. Hillebrecht, Z. Zolnierek, R. Lässer, Ch. Freiburg, O. Gunnarsson, and K. Schönhammer, Phys. Rev. B **27**, 7330 (1983).
[51] F.U. Hillebrecht, J.C. Fuggle, G.A. Sawatzky, and R. Zeller, Phys. Rev. Lett. **51**, 1187 (1983).
[52] L. Braicovich, L. Duò, P. Vavassori, and G.L. Olcese, Surf. Sci. **331-333**, 782 (1995).
[53] E. Beaurepaire, J.P. Kappler, S. Lewonczuk, J. Ringeisen, M.A. Kahn, J.C. Parlebas, Y. Iwamoto, and A. Kotani, J. Phys.: Condens. Matter **5**, 5841 (1993); Y. Iwamoto, M. Nakazawa, A. Kotani, and J.C. Parlebas, *ibid.* **7**, 1149 (1995).
[54] R.A. Neifeld, M. Croft, T. Mihalisin, C.U. Segre, M. Madigan, M. Torikachvili, M.B. Maple, and L.E. DeLong, Phys. Rev. B **39**, 6928 (1985).
[55] G.L. Olcese, J. Phys. (Paris) Colloq. **40**, C5-334 (1979).
[56] P. Weidner, K. Keulerz, R. Löhe, B. Roden, J. Röhler, B. Wittershagen, and D. Wohlleben, J. Magn. Magn. Mater. **47&48**, 75 (1985).
[57] L. Severin and B. Johansson, Phys. Rev. B **50**, 17 886 (1994).
[58] E. Weschke, C. Laubschat, R. Ecker, A. Höhr, M. Domke, G. Kaindl, L. Severin, and B. Johansson, Phys. Rev. Lett. **69**, 1792 (1992).
[59] B.T. Thole, G. van der Laan, J.C. Fuggle, G.A. Sawatzky, R.C. Karnatak, and J.M. Esteva, Phys. Rev. B **32**, 5107 (1985).
[60] P.Weibel, M. Grioni, D. Malterre, O. Manzardo, Y. Baer, and G.L. Olcese, Europhys. Lett. **29**, 629 (1995).
[61] O. Gunnarsson and K. Schönhammer, in *Handbook on the Phys-*

ics and Chemistry of the Rare Earths, edited by K.A. Gschneidner, Jr., L. Eyring, and S. Hüfner (North-Holland, Amsterdam, 1987), Vol. 10, p. 103.

[62] L.H. Tjeng, S.-J. Oh, E.-J. Cho, H.-J. Lin, C.T. Chen, G.-H. Gweon, J.-H. Park, J.W. Allen, T. Suzuki, M.S. Makivich, and D.L. Cox, Phys. Rev. Lett. **71**, 1419 (1993).

[63] P. Weibel, M. Grioni, M. Malterre, B. Dardel, Y. Baer, and M.L. Besnus, Z. Phys. B **91**, 337 (1993).

[64] R.I.R. Blyth, J.J. Joyce, A.J. Arko, P.C. Canfield, A.B. Andrews, Z. Fisk, J.D. Thompson, R.J. Barlett, P. Riseborough, J. Tang, and J.M. Lawrence, Phys. Rev. B **48**, 9497 (1993).

[65] D. Malterre, M. Grioni, P. Weibel, B. Dardel, and Y. Baer, Phys. Rev. Lett. **68**, 2656 (1992).

[66] D. Malterre, M. Grioni, P. Weibel, B. Dardel, and Y. Baer, Europhys. Lett. **20**, 445 (1992).